Supplementary Information

Thermoelectric performance of 2D materials: band-convergent strategy and strong intervalley scatterings

Yu Wu,[1] Bowen Hou,[1] Congcong Ma,[2] Jiang Cao,[3] Ying Chen,[2]
Zixuan Lu,[2] Haodong Mei,[1] Hezhu Shao,[4] Yuanfeng Xu,[5,†]
Heyuan Zhu,[1] Zhilai Fang,[2] Rongjun Zhang,[1,‡] and Hao Zhang[1,6,*]

[1]*Key Laboratory of Micro and Nano Photonic Structures (MOE) and Key Laboratory for Information Science of Electromagnetic Waves (MOE) and Department of Optical Science and Engineering, Fudan University, Shanghai 200433, China*

[2]*Department of Light Sources and Illuminating Engineering, and Academy for Engineering & Technology, Fudan University, Shanghai, 200433, China*

[3]*School of Electronic and Optical Engineering, Nanjing University of Science and Technology, Nanjing 210094, China*

[4]*College of Electrical and Electronic Engineering, Wenzhou University, Wenzhou, 325035, China*

[5]*School of Science, Shandong Jianzhu University, Jinan 250101, Shandong, China*

[6]*Nanjing University, National Laboratory of Solid State Microstructure, Nanjing 210093, China*

I. THE OPTIMIZED STRUCTURES OF β- AND α-SB

The top and side views of optimized conficuration of antimonene allotropes are shown in Fig. S1. The β-Sb has a honeycomblike structure and a buckled surface with optimized lattice constant $a = 4.12$ Å. The bond length of the neighbouring Sb-Sb atoms is $d = 2.89$ Å and the bond angle is 90.83°. The structure has two atomic planes with three atoms at the corners of the hexagon raised while the ramaining atoms lowered. By buckling, the weaker planner sp^2 bonding is dehybridized to form sp^3-like hybridization to enhance the stability of the structure[1].

II. THE ELECTRONIC BANDSTRUCTURES AND PHONON DISPERSION CURVES OF β- AND α-SB

The electronic bands of the two structures are shown in Fig. S2(a,b). For a better understanding of atomic orbital contributions, the band structures are projected by the atomic orbitals of the Sb atom. β-Sb monolayer is a semiconductor with an indirect band gap of 1.26 eV with the valence band maximum (VBM) located at Γ point while the conduction band minimum (CBM) along the Γ-M direction. Compared with graphene, the electronic bands of which near the Fermi level are mainly composed of pz orbitals of C atom, the VBM of β-Sb is dominantly contributed from px and py orbitals while px and pz orbitals for the CBM due to the bumpy structure. The formed covalent σ bonds from sp^3-like hybridization provide the rigidity of β-Sb. For α-Sb, it has a relatively small direct band gap of $\sim$ 0.20 eV. The VBM and CBM are mainly contributed from the py and s orbitals of Sb atom, which form an almost linear dispersion band structure beneficial to the carrier transport. It is worth noting that the conduction bands of β-Sb and α-Sb have a multivalley character which will play an important role in intervalley scattering.

Fig. S3 shows contour map of the conduction band of monolayer (a) β-Sb and (b) α-Sb in the first Brillouin zone. We can find that multivalleys appear in the bandstructures of β-Sb and α-Sb which can favor intervalley scattering. For β-Sb, the conduction band exhibits six-fold rotation symmetry the CBM is along Γ-M direction which shows evident anisotropy than the Γ point.The conduction band of α-Sb shows two-fold rotation symmetry and more complicated valley system. The CBM is along the Γ-Y direction and the band near CBM exhibits linear property and large anisotropy.

The calculated phonon dispersions for β-Sb and α-Sb are shown in Fig. S2(c,d), and no imag-

inary frequencies can be found in both phonon dispersions which indicate their good thermodynamic stabilities at low temperatures. The maximum phonon energies for β-Sb and α-Sb are 20.90 meV and 20.92 meV respectively, and both monolayers possess phonon bandgaps around 13.0 meV with the respective values of 7.96 meV and 3.27 meV.

III. THE SCATTERING RATES FOR HOLES OF β-SB

To investigate the behavior of holes in β-Sb, Fig. S4 exhibits the scattering rate near Γ point within $\sim$ 0.20 eV below the VBM. Contrary to the general conclusion that the carriers (electrons and holes) in material with D_{3d} symmetry will suffer from ZA phonon scattering most, which has been verified in all the group-IV elemental materials (Silicene, Silicene, Stanene), the scattering of holes mainly comes from LA phonons in β-Sb

IV. METHOD OF SEPARATINNG INTRAVALLEY AND INTERVALLEY SCATTERING RATES

Since the phonons involved in the intravalley scatterings possess small momenta, in the calculations for intravalley scatterings, only phonons with q points uniformly distributed in a small region are considered. Fig. S5 shows the electron-phonon scattering rates for CBM electrons for β- and α-Sb respectively with different meshes of q points, which reveals that, when the size of the small region increases, the obtained electron-phonon scattering rates reach a convergent value, meaning that, the major part of the phonons with small momenta involved in the intravalley scatterings are considered. In this work, the size of the q mesh is chosen as 0.08 for both β- and α-Sb monolayers.

V. AIMD SIMULATION FOR β- AND α-SB AT DIFFERENT TEMPERATURES

We also carry out the *ab initio* molecule dynamics (AIMD) simulation to study the thermal stability of monolayer aw-Sb at high temperatures. The AIMD simulation results shown in Fig. S6 verify that, aw-Sb monolayer remains stable up to at least 600 K. But when the temperature increases to 800 K, some bonds break which means that the original structure is no longer stable due to thermal excitations.

VI. SELECTION RULE FOR β-SB AND SN

In order to understand the physics behind scattering rate, we emoloyed selection rules in terms of materials symmetry to calculate allowed phonon modes involved in electron-phonon scattering process. Table S1 gives the irreps for acoustic phonon modes, initial and final states. The selection rules of intra-valley electron-phonon interation for monolayer Sn have good agreement with previous study[2]. Table S2 gives the selection rules for scattering rate occuring between degenerates CBM or VBM in Brillouin zone.

VII. THE SCATTERING RATES OF CARRIERS OF α-SB

In order to view the contribution of different phonon modes to the electron scattering clearly, the scattering rate of electrons in the conduction band of α-Sb as a function of wave vector **k** in Cartesian coordinate at the first Brillouin zone are shown in Fig. S7.

Fig. S8 shows the scattering of holes in the peak along Γ-Y direction within $\sim$ 0.4 eV below the VBM. The LA and LO1 phonons contribute to the intravalley scattering most. It is clear that the variation range of the vertical axis is much less than the case of conduction band which is due to the greater energy difference of peaks in the valence band and the intervalley scattering is forbidden.

Table S3 shows the resloved scattering rates coming from scattering between different valleys and the total value including the intravalley scattering. The initial state is chosen as (0, 0.323, 0) in Fractional coordinates). The I-J, I-K and I-L intervalley scatterings take up considerable proportion of the total scattering with 4.4%, 29.9% and 9.7%, respectively.

VIII. PHONON LINEWIDTH OF α-SB

The obtained phonon linewidth for α-Sb is shown in Fig. S10. We can find that only the phonons at high energy level near Γ point experience evident scattering from carriers, indicating the scattering is mainly from the interband transition of electrons.

IX. THE CARRIER MOBILITIES CALCULATED BY USING TWO DPA METHODS

The carrier mobility can be calculated according to the deformation-potential theory which only considers the coupling between electrons and longitudial phonons and is widely used in semiconductors,

$$\mu^{2D} = \frac{2e\hbar^3 C^{2D}}{3k_B T m^{*2} E_l^2} \tag{S1}$$

Where e is the electron charge, $\hbar$ is the reduced Planck's constant, T is the temperature set as 300K in this paper. C^{2D} is the elastic modulus derived from $C^{2D} = [\partial^2 E/\partial(\Delta l/l_0)^2]/S_0$, where E is the total energy and Δl is the change in lattice constant and S_0 is the area of the equilibrium supercell. m^* is the effective mass obtained by $m^* = \hbar^2(\partial^2 E(k)/\partial(k)^2)^{-1}$. The contribution of phonon scattering to the carriers is included in the deformation potential constant E_l, defined as $\Delta E_{CBM(VBM)}/(\Delta l/l_0)$, in which $\Delta E_{CBM(VBM)}$ is the shift of the VBM and CBM with respect to the lattice deformation Δl.

Howerver, Eq S1 indicates that the mobility in a specified direction is determined only by C and E_l in the same direction but is independent of those in the perpendicular direction. To reasonably use deformation potential theory to calculate the carrier mobility of anisotropic 2D semiconductors, a modified method has been proposed[3],

$$\mu_x = \frac{e\hbar^3}{k_B T\,(m_x)^{\frac{3}{2}}\left(m_y\right)^{\frac{1}{2}}}\left(\frac{A+B-\sqrt{A^2-B^2}}{B\sqrt{A^2-B^2}}\right)\times\left(\frac{I+J-\sqrt{I^2-J^2}}{J\sqrt{I^2-J^2}}\right) \tag{S2}$$

where $A = \bar{E}_l^2 + \frac{(\Delta E_l)^2}{2}$, $B = \bar{E}_l \Delta E_l$, $I = \frac{1}{\sqrt{\bar{C}^2-(\Delta C)^2}}$ and $J = \frac{\bar{C}}{\Delta C}\left(\frac{1}{\bar{C}} - \frac{1}{\sqrt{\bar{C}^2-(\Delta C)^2}}\right)$ with $\bar{E}_l = \frac{E_{ly}+E_{lx}}{2}$, $\Delta E_1 = \frac{E_{ly}-E_{lx}}{2}$, $\bar{C} = \frac{C_x+C_y}{2}$ and $\Delta C = \frac{C_y-C_x}{2}$.

The carrier mobilities and relaxation time for β- and α-Sb under these two DPA methods are listed in TABLE S4. It is clear that the results under modified DPA method is more close to the full electron-phonon coupling results and the the anisotropy in α-Sb system is weaker than previously thought.

X. THE INTRAVALLEY SCATTERING LIMITED CARRIER MOBILITIES

The carrier mobilities of β- and α-Sb by taking into account full electron-phonon couplings and only intravalley scatterings are shown in Fig. S9. For β-Sb monolayer, the electron mobility

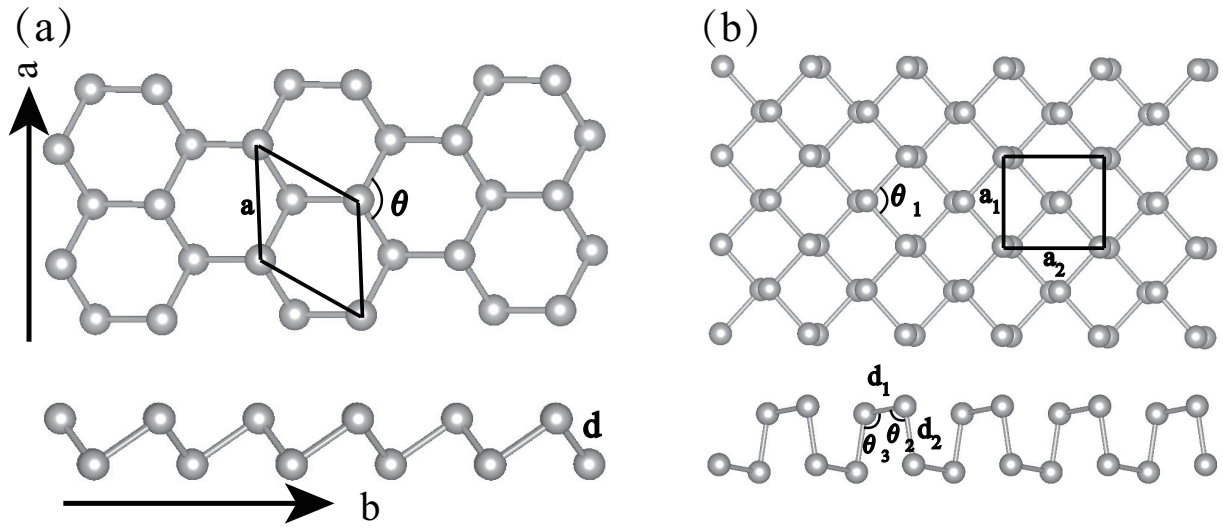

FIG. S1: Atomic structure of monolayer (a) β-Sb and (b) α-Sb from top view and side view.

TABLE S1: The irreducible representations for initial states and final states of transitional electrons and three acoustic phonon modes, which involve in intra-valley electron-phonon intercation within conduction and valence band valley in monolayerSn and β-Sb.

		Γ_i	Γ_{ZA}	Γ_{TA}	Γ_{LA}	Γ_f	Selection Rules	
Sn	i=C_1' f=C_1'	A	B	B	A	B	ZA TA	ZA^2 TA^2
		Γ-K (C_2)	Γ-K (C_2)	Γ-K(C_2)	Γ-K(C_2)	M-K(C_2)		
β-Sb	i=C_1' f=C_1'	A'	A'	A"	A'	A'	ZA LA	
		Γ-M (C_S)	Γ-M (C_S)	Γ-M(C_S)	Γ-M(C_S)	Γ-M(C_S)		
Sn	i=V_1' f=V_1'	A	B	B	A	B	ZA TA	ZA^2 TA^2
		M-K (C_2)	Γ-K (C_2)	Γ-K(C_2)	Γ-K(C_2)	Γ-K(C_2)		
β-Sb	i=V_1' f=V_1'	A	B	B	A	A	LA	
		Γ-M (C_2)	Γ-K (C_2)	Γ-K(C_2)	Γ-K(C_2)	Γ-M(C_2)		

decreases by nearly 7 times at 300 K when full electron-phonon coupling considered, but the hole mobility almost does not change. For α-Sb monolayer, the calculated mobilities considering only intravalley scatterings are 2∼4 times larger than those considering full electron-phonon couplings at 300 K.

XI. THE TE PERFORMANCE OF α-SB ALONG b DIRECTION

The TE performance of α-Sb along b direction is shown in Fig. S11. We can find that near $E_f = 0$, the σ and κ under CRTA method is in good agreement with the full electron-phonon coupling results and the calculated zT is very close to each other.

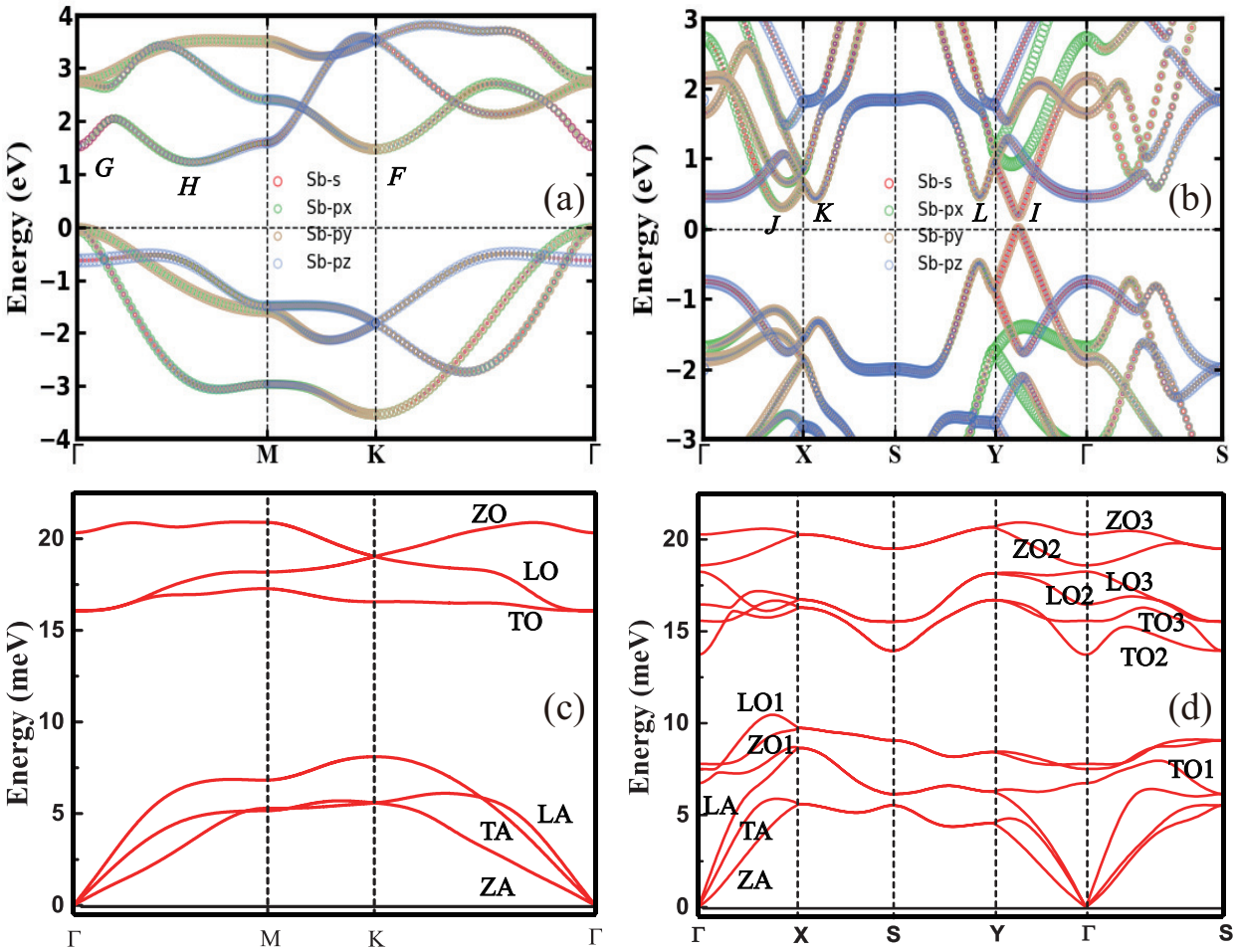

FIG. S2: The electronic band structure and phonon dispersion relation of (a,c) β-Sb and (b,d) α-Sb.

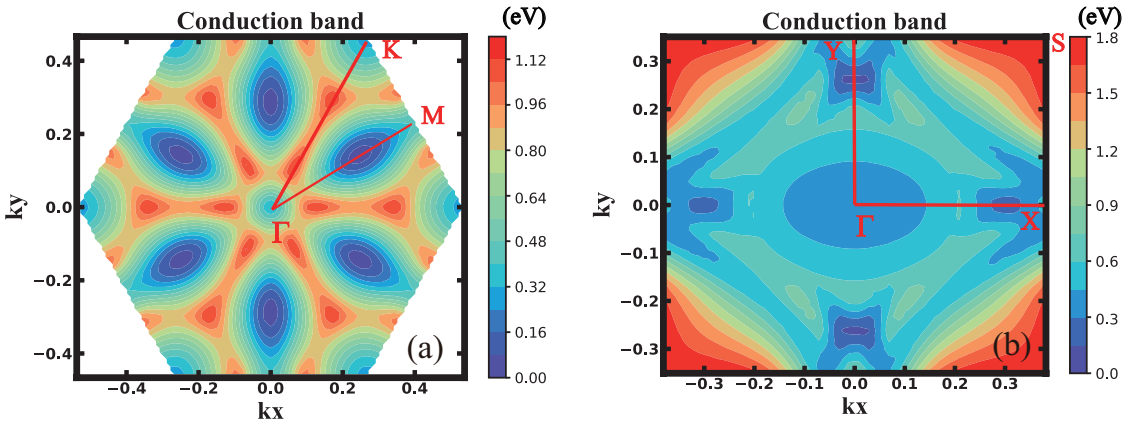

FIG. S3: Contour map of the conduction band of monolayer (a) β-Sb and (b) α-Sb in the first Brillouin zone in Cartesian coordinate.

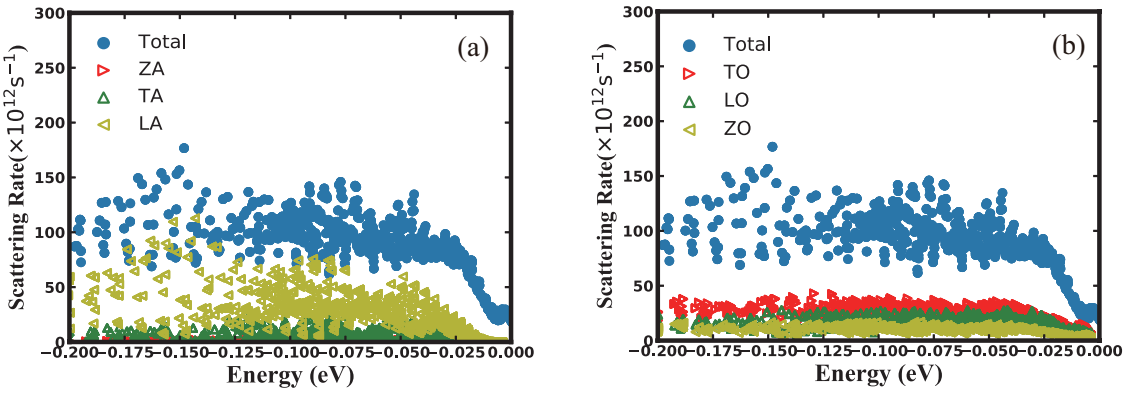

FIG. S4: The scattering rate of holes in the peak near Γ point with energies within ~ 0.2 eV below the VBM. (a) The contributions of acoustic branch phonons to the total scattering rate. (b) The contributions of optical branch phonons to the total scattering rate.

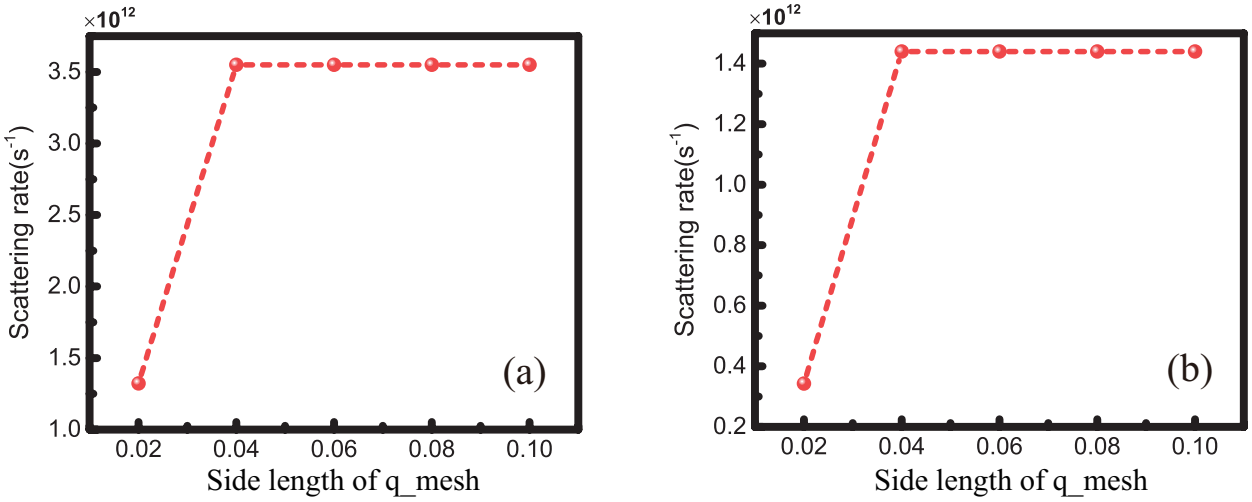

FIG. S5: The calculated intravalley scattering rate at CBM with different q mesh for (a) β- and (b) α-Sb, respectively.

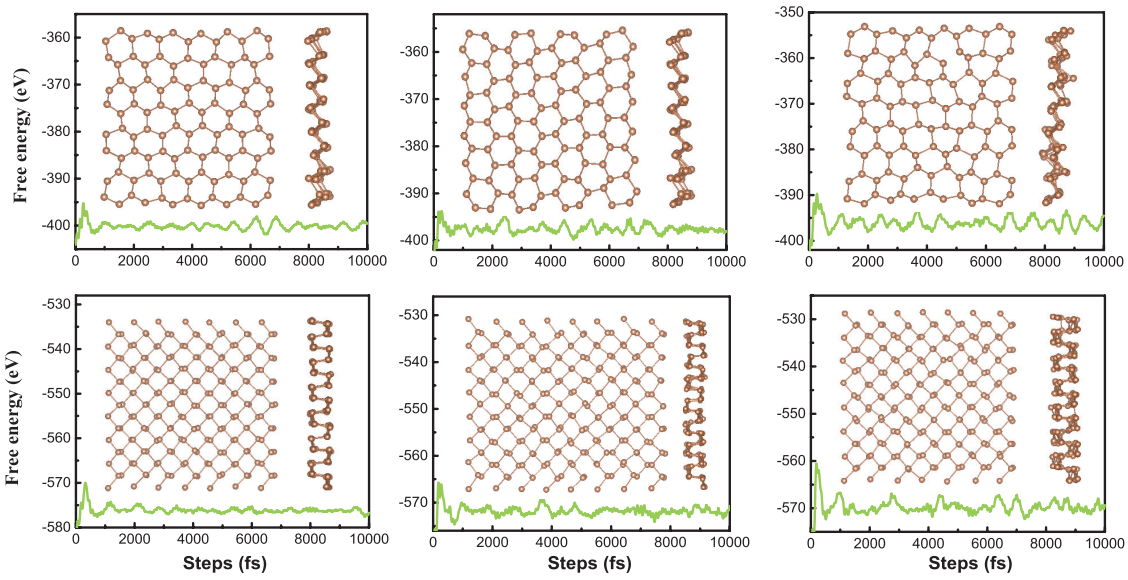

FIG. S6: The snapshot of the atomic configuration obtained by AMID calculations at 300 K, 500 K and 600 K for monolayer (a,b,c) β-Sb and (d,e,f) α-Sb. The green curve indicates the fluctuation of the total energy at at different time with a time interval of 2 fs and a total simulation time of 10 ps.

TABLE S2: The irreducible representations for initial states final states of transitional electrons and three acoustic phonon modes which involve in inter-valley electron-phonon intercation between degenerate C_1 or V_1 valleys in monolayer β-Sb and Sn.

		Γ_i	Γ_{ZA}	Γ_{TA}	Γ_{LA}	Γ_f	Selection Rules
Sn	i=C_1' f=C_1"	B	B	A	B	B	TA
		M-K (C_2)	Γ-K (C_2)	Γ-K(C_2)	Γ-K(C_2)	M-K(C_2)	
	i=C_1' f=C_1"'	A	B	A	B	A	TA
		Γ-K (C_2)	Γ-K (C_2)	Γ-K(C_2)	Γ-K(C_2)	Γ-K(C_2)	
	i=V_1' f=V_1"	A	B	A	B	A	TA
		M-K (C_2)	Γ-K (C_2)	Γ-K(C_2)	Γ-K(C_2)	M-K(C_2)	
	i=V_1' f=V_1"'	B	B	A	B	B	TA
		Γ-K (C_2)	Γ-K (C_2)	Γ-K(C_2)	Γ-K(C_2)	Γ-K(C_2)	
β-Sb	i=C_1' f=C_1"	A'	A'	A"	A'	A'	ZA LA
		Γ-M (C_S)	Γ-M (C_S)	Γ-M(C_S)	Γ-M(C_S)	Γ-M(C_S)	
	i=C_1' f=C_1"'	A'	A'	A"	A'	A'	ZA LA
		Γ-M (C_S)	Γ-M (C_S)	Γ-M(C_S)	Γ-M(C_S)	Γ-M(C_S)	

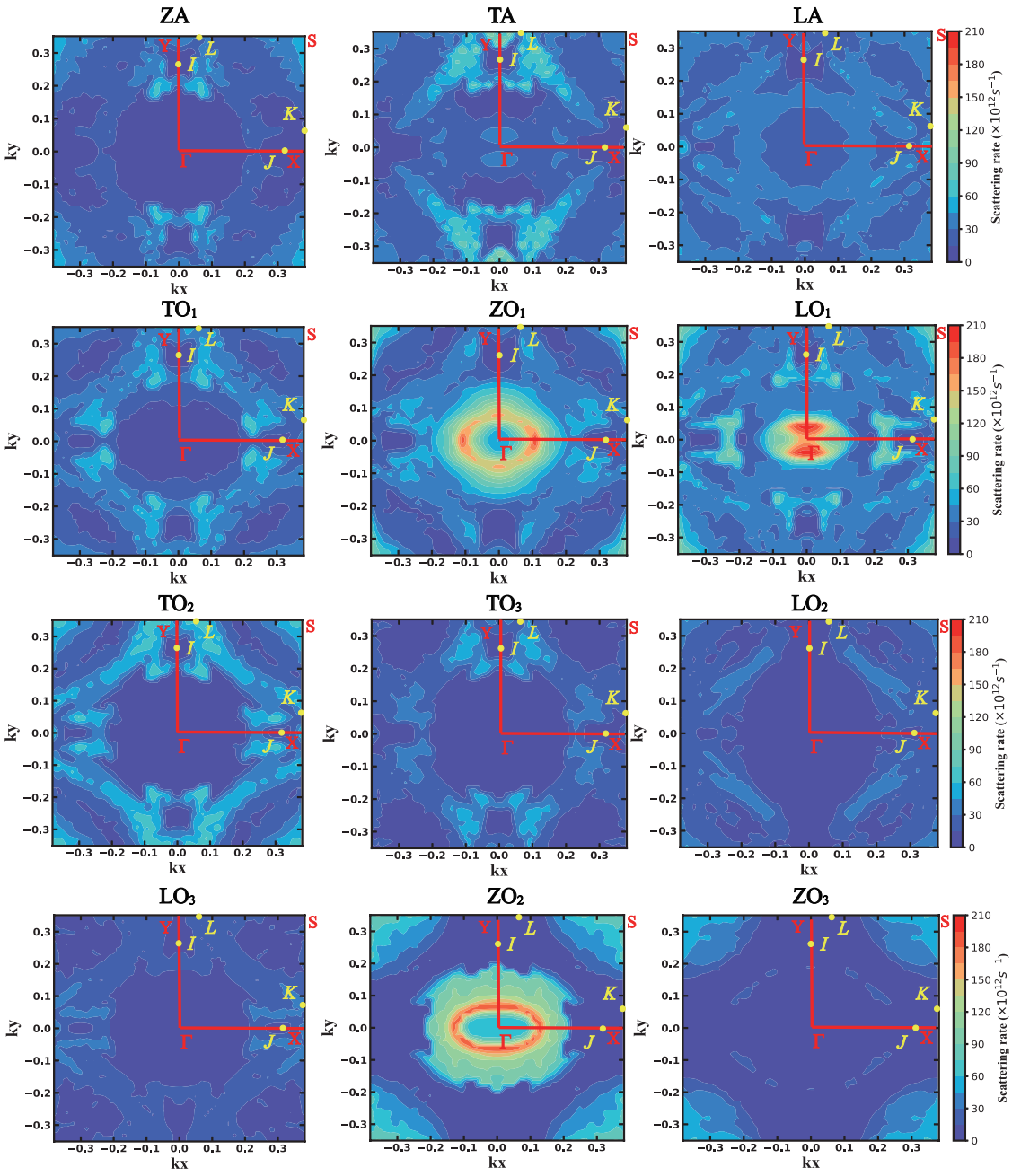

FIG. S7: The scattering rate of electrons in the conduction band for α-Sb as a function of wave vector **k** at first Brillouin zone.

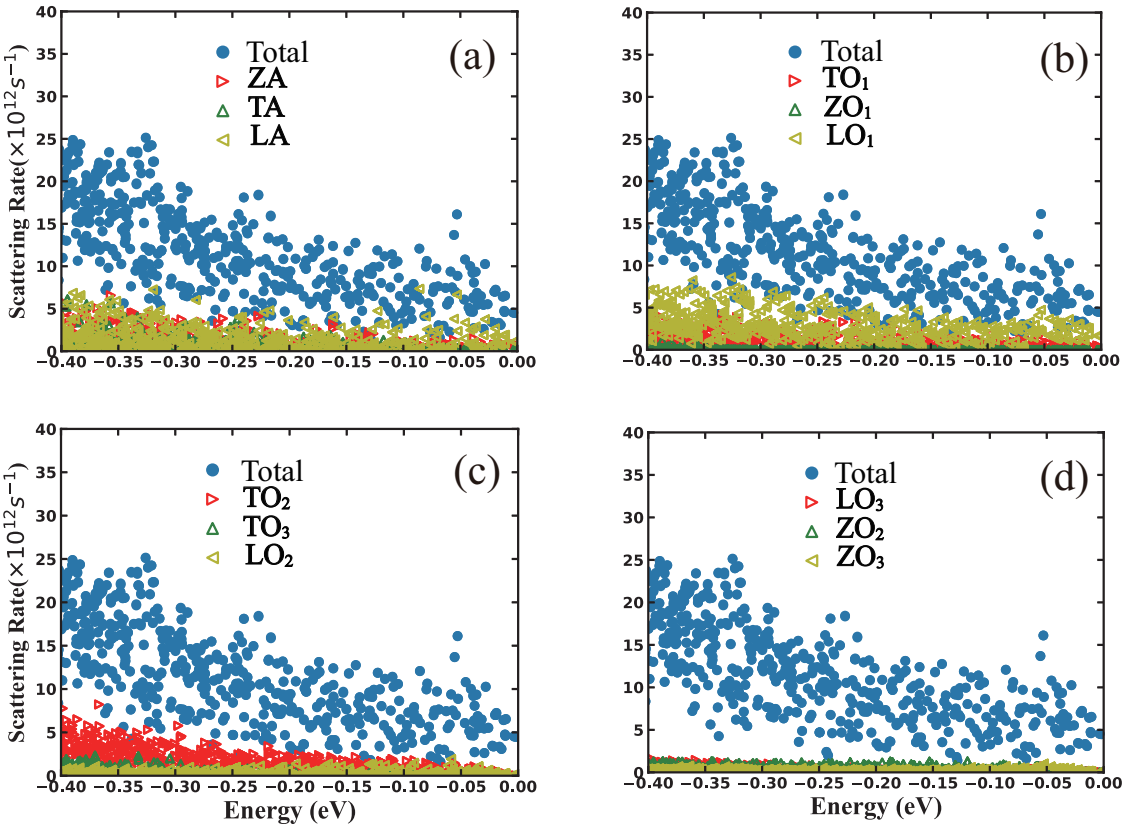

FIG. S8: The scattering rate of holes in the peak along Γ-Y direction with energies within ~ 0.4 eV below the VBM. (a) The contributions of acoustic branch phonons to the total scattering rate. (b,c,d) The contributions of optical branch phonons to the total scattering rate.

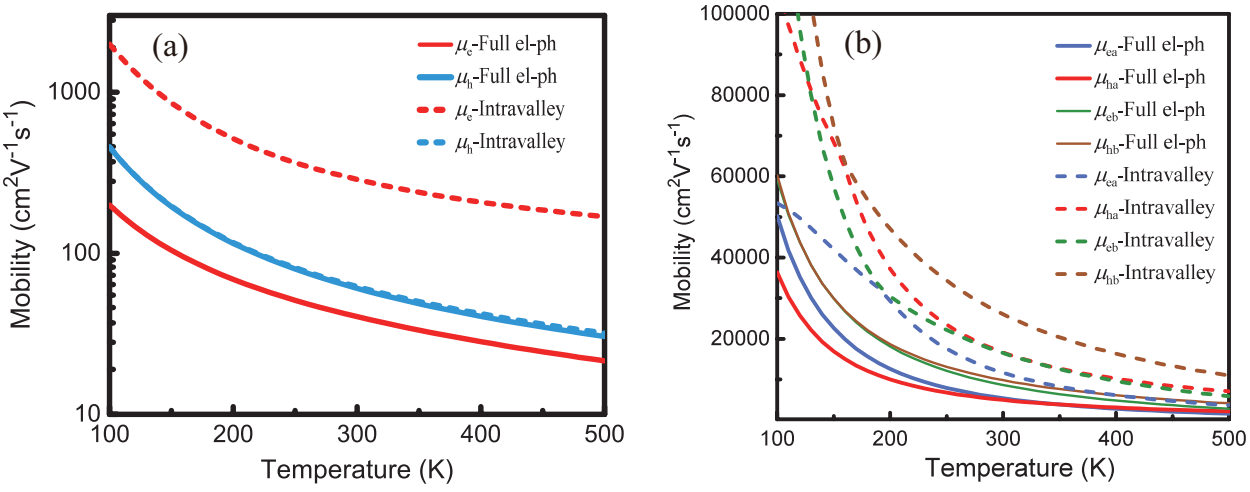

FIG. S9: Carrier mobilities calculated using the full electron-phonon coupling scattering rates and considering only intravalley scattering for (a) β- and (b) α-Sb, respectively.

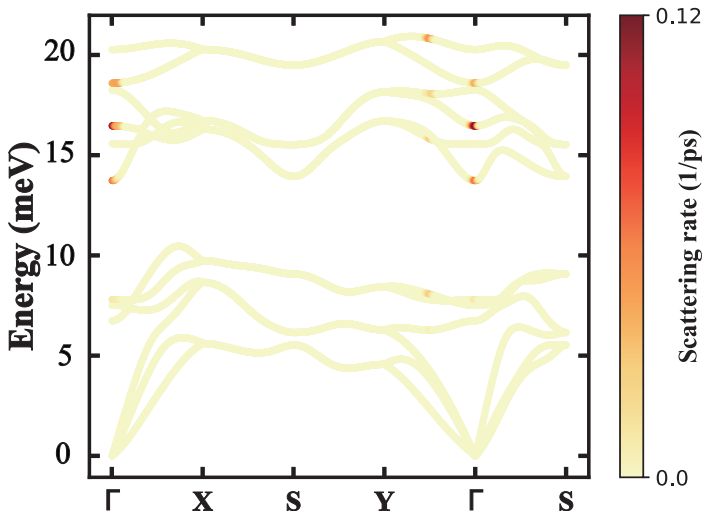

FIG. S10: Calculated phonon dispersion curve along the high symmetry directions for α-Sb. The color code shows the calculated scattering rates of phonons caused by excited electrons in the conduction band.

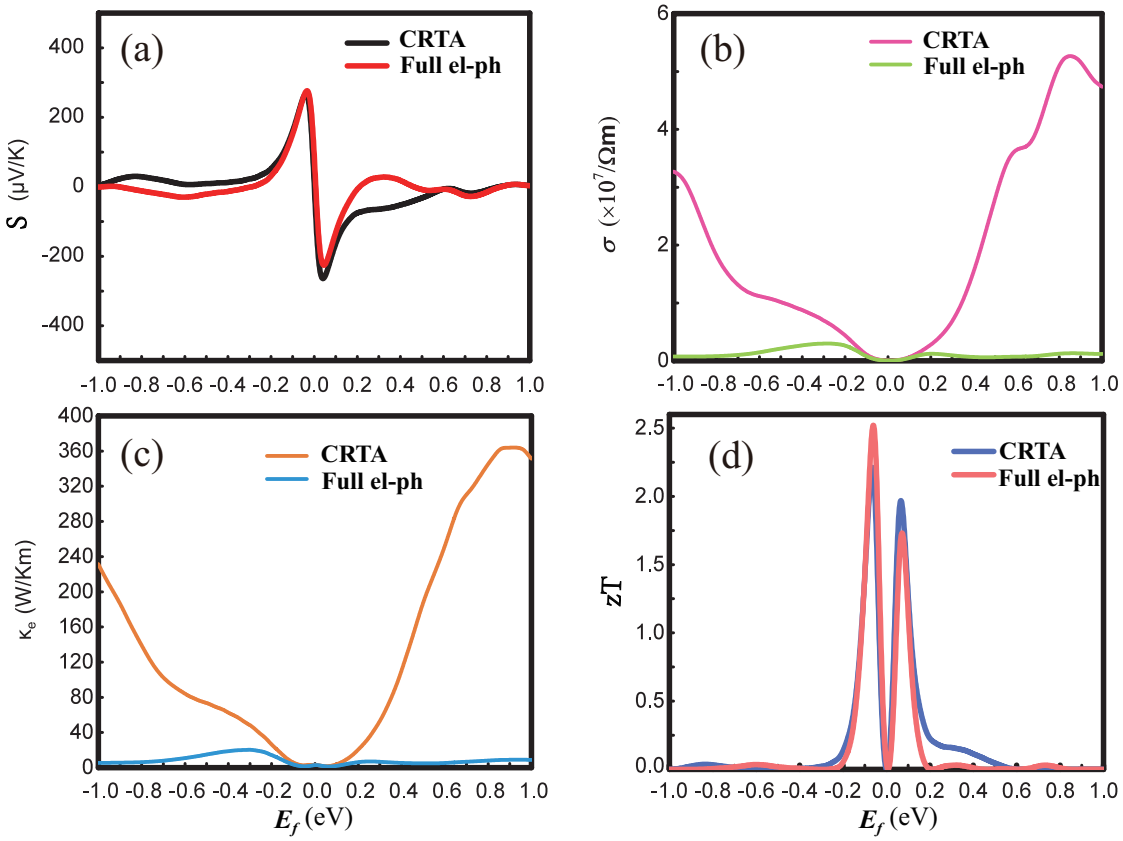

FIG. S11: The (a) seebeck coefficients (b) electrical conductivity (c) electronic thermal conductivity and (d) zT value as a function of chemical potential at 300 K for α-Sb along b direction.

TABLE S3: Inter-valley scattering between I-J, I-K and I-L for electrons in α-Sb at (0, 0.323, 0) point and T = 300 K.

Phonon mode	I-J (s^{-1})	I-K (s^{-1})	I-L (s^{-1})	Total (s^{-1})
ZA	4.95×10^{11}	5.19×10^{12}	3.05×10^{12}	4.29×10^{13}
TA	9.39×10^{11}	2.84×10^{12}	3.41×10^{12}	2.02×10^{13}
LA	6.73×10^{11}	6.55×10^{12}	7.64×10^{11}	1.05×10^{13}
TO_1	2.66×10^{11}	6.01×10^{12}	6.84×10^{11}	1.16×10^{13}
ZO_1	4.86×10^{10}	1.69×10^{12}	1.12×10^{12}	6.72×10^{12}
LO_1	3.50×10^{11}	2.06×10^{12}	1.57×10^{12}	3.51×10^{13}
TO_2	1.30×10^{12}	4.71×10^{12}	2.37×10^{12}	1.24×10^{13}
TO_3	1.23×10^{12}	2.28×10^{13}	4.99×10^{12}	3.23×10^{13}
LO_2	2.63×10^{11}	3.02×10^{12}	1.38×10^{12}	6.97×10^{12}
LO_3	3.45×10^{12}	5.83×10^{12}	4.59×10^{11}	1.90×10^{13}
ZO_2	4.64×10^{11}	2.30×10^{12}	4.21×10^{11}	4.15×10^{12}
ZO_3	6.27×10^{10}	1.46×10^{12}	7.94×10^{11}	1.34×10^{13}
Sum	9.55×10^{12}	6.44×10^{13}	2.10×10^{13}	2.15×10^{14}
Ratio	4.4%	29.9%	9.7%	100%

TABLE S4: Calculated effective mass m, deformation potential constant E_l, 2D elastic modulus C,carrier mobility μ and relation time τ along a and b directions using old and modified DPA theory.

Direction	Carrier type	Effective mass(m_0)	E_l(eV)	C^{2D}(J/m^2)	old-μ(cm^2/V $\cdot$ s)	old-τ(ps)	new-μ(cm^2/V $\cdot$ s)	new-τ(ps)	
α-Sb	a	electron	0.138	6.20	45.95	887.09	0.07	2125.62	0.17
a	hole	0.118	8.75	45.95	607.05	0.04	2593.66	0.17	
b	electron	0.038	4.45	14.54	7225.88	0.16	6818.51	0.15	
b	hole	0.025	1.56	14.54	135846.61	1.93	17313.09	0.25	
β-Sb	a	electron	0.14	6.95	31.15	467.57	0.04	785.27	0.06
a	hole	0.48	3.98	31.15	121.29	0.03	190.25	0.05	
b	electron	0.42	1.27	31.40	1568.32	0.37	492.30	0.12	
b	hole	0.45	3.93	31.40	142.67	0.04	204.63	0.05	

† Electronic address: xuyuanfeng19@sdjzu.edu.cn

‡ Electronic address: rjzhang@fudan.edu.cn

* Electronic address: zhangh@fudan.edu.cn

[1] E. Akturk, O. U. Akturk, and S. Ciraci, PHYSICAL REVIEW B **94** (2016), ISSN 2469-9950.

[2] Y. Nakamura, T. Zhao, J. Xi, W. Shi, D. Wang, and Z. Shuai, Advanced Electronic Materials **3**, 1700143 (2017).

[3] H. Lang, S. Zhang, and Z. Liu, Physical Review B **94** (2016).